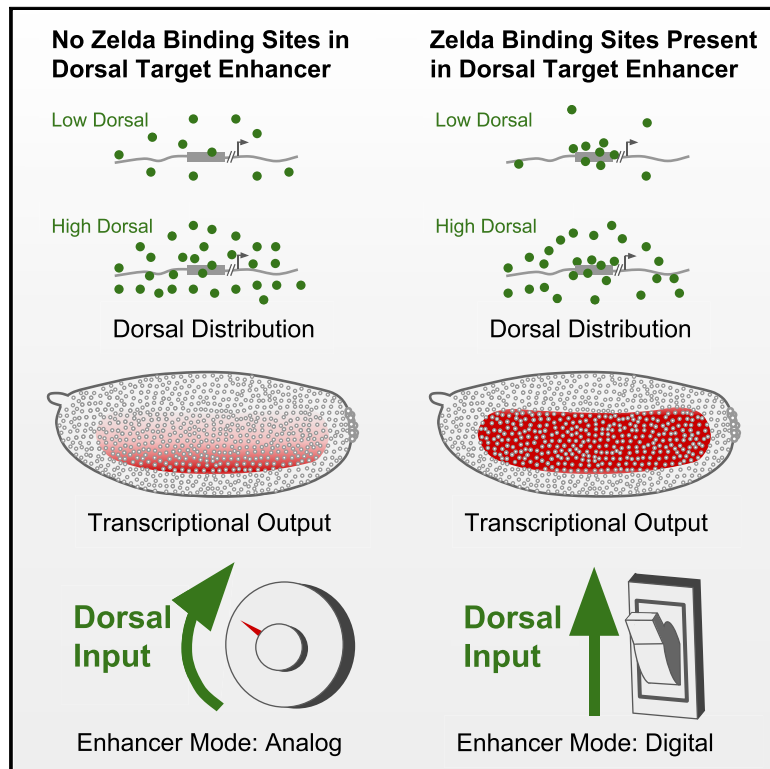


Current Biology

The *Drosophila* Pioneer Factor Zelda Modulates the Nuclear Microenvironment of a Dorsal Target Enhancer to Potentiate Transcriptional Output

Graphical Abstract



Authors

Shigehiro Yamada, Peter H. Whitney, Shao-Kuei Huang, Elizabeth C. Eck, Hernan G. Garcia, Christine A. Rushlow

Correspondence

chris.rushlow@nyu.edu

In Brief

Drosophila embryos establish a graded distribution of Dorsal protein to define the dorsal-ventral axis in early development. Yamada, Whitney, et al. demonstrate how Zelda allows a *cis*-regulatory element to unify gene expression over a broad dynamic range of the Dorsal gradient by raising the local concentration of Dorsal at the enhancer.

Highlights

- The expression domain of the Dorsal target gene *sog* narrows in the absence of Zelda
- Using MS2 reporter transgenes, this can be accurately recapitulated in living embryos
- Without Zelda, the onset and degree of reporter activation becomes graded like Dorsal
- Zelda promotes accumulation of Dorsal protein at the site of the enhancer



The *Drosophila* Pioneer Factor Zelda Modulates the Nuclear Microenvironment of a Dorsal Target Enhancer to Potentiate Transcriptional Output

Shigehiro Yamada,^{1,6} Peter H. Whitney,^{1,6} Shao-Kuei Huang,¹ Elizabeth C. Eck,² Hernan G. Garcia,^{2,3,4,5} and Christine A. Rushlow^{1,7,*}

¹Department of Biology, New York University, New York, NY 10003, USA

²Biophysics Graduate Group, University of California at Berkeley, Berkeley, CA 94720, USA

³Department of Molecular and Cellular Biology, University of California at Berkeley, Berkeley, CA 94720, USA

⁴Department of Physics, University of California at Berkeley, Berkeley, CA 94720, USA

⁵Quantitative Biosciences-QB3, University of California at Berkeley, Berkeley, CA 94720, USA

⁶These authors contributed equally

⁷Lead Contact

*Correspondence: chris.rushlow@nyu.edu

<https://doi.org/10.1016/j.cub.2019.03.019>

SUMMARY

Connecting the developmental patterning of tissues to the mechanistic control of RNA polymerase II remains a long-term goal of developmental biology. Many key elements have been identified in the establishment of spatial-temporal control of transcription in the early *Drosophila* embryo, a model system for transcriptional regulation. The dorsal-ventral axis of the *Drosophila* embryo is determined by the graded distribution of Dorsal (DI), a homolog of the nuclear factor κ B (NF- κ B) family of transcriptional activators found in humans [1, 2]. A second maternally deposited factor, Zelda (Zld), is uniformly distributed in the embryo and is thought to act as a pioneer factor, increasing enhancer accessibility for transcription factors, such as DI [3–9]. Here, we utilized the MS2 live imaging system to evaluate the expression of the DI target gene *short gastrulation* (*sog*) to better understand how a pioneer factor affects the kinetic parameters of transcription. Our experiments indicate that Zld modifies probability of activation, the timing of this activation, and the rate at which transcription occurs. Our results further show that this effective rate increase is due to an increased accumulation of DI at the site of transcription, suggesting that transcription factor “hubs” induced by Zld [10] functionally regulate transcription.

RESULTS

Our study focused on the Dorsal (DI) target gene *sog*, as its expression domain spans a large dynamic range of the DI gradient, allowing us to examine how Zelda (Zld) potentiates DI activity across the dorsal-ventral axis. Previous experiments have demonstrated that the lateral stripe of *sog* expression narrows dramatically in *zld*-null embryos [5, 11] (Figures 1A and 1B)

and that progressively removing Zld DNA binding sites from the *sog* shadow (distal) enhancer shrinks the domain of activation of reporter genes in a linear manner [7]. In order to understand how Zld influences transcription at different points along the DI gradient, we revisited these constructs with the aim of visualizing transcription in real time by adding 24 MS2 loops to the 5' end of the *lacZ* reporter. Because previously utilized MS2 loops [12–15] contained potential Zld binding sites [16], we revised the MS2v5 [17] sequence to make a Zld binding-site-free non-repetitive version, referred to as MS2v5(-TAG) (see STAR Methods). Constructs also contained either the *sog* shadow (distal) enhancer [18, 19] with its three native canonical Zld binding sites, CAGGTAG (hereafter referred to as “3TAG”), or without these sites (hereafter referred to as “0TAG”; Figure 1C; see STAR Methods for enhancer sequences) [7]. The narrowing effect of removing Zld binding sites was confirmed by *in situ* hybridization (Figures 1D and 1E).

By crossing these transgenic reporter lines to females expressing the MCP (MS2 coat protein)-GFP fusion gene during oogenesis [14], we visualized the transcriptional activation of each reporter as fluorescent foci (see Figure 1C and STAR Methods). These embryos also express H2Av(histone 2A variant)-RFP [20], allowing us to track nuclear cycles and record transcriptional activation events in space and time. We performed confocal live imaging over the course of nuclear cycles 10–14 (NC10–NC14), tracking the activation of the 3TAG and 0TAG reporter genes (Videos S1 and S2). To validate that the MS2 transgenes behaved as expected, we examined transcriptional activation events in space and time and compared those to expression as assessed by conventional *in situ* analysis. We find that the 3TAG construct is activated as early as NC10, although activation of the 0TAG construct is delayed until NC11 or NC12 (Figures 2A and 2B; Videos S1 and S2; also see additional Videos S3, S4, S5, and S6), in agreement with previously published results of *sog* activation in *zld* mutants [5].

To compare the spatial differences in activation, we divided the expression domain of *sog* into five discrete zones, with zone 1 comprising the mesoderm and all subsequent zones defined by 20- μ m-width bands moving sequentially toward the dorsal midline of the embryo, diagrammed in Figure 2C. The



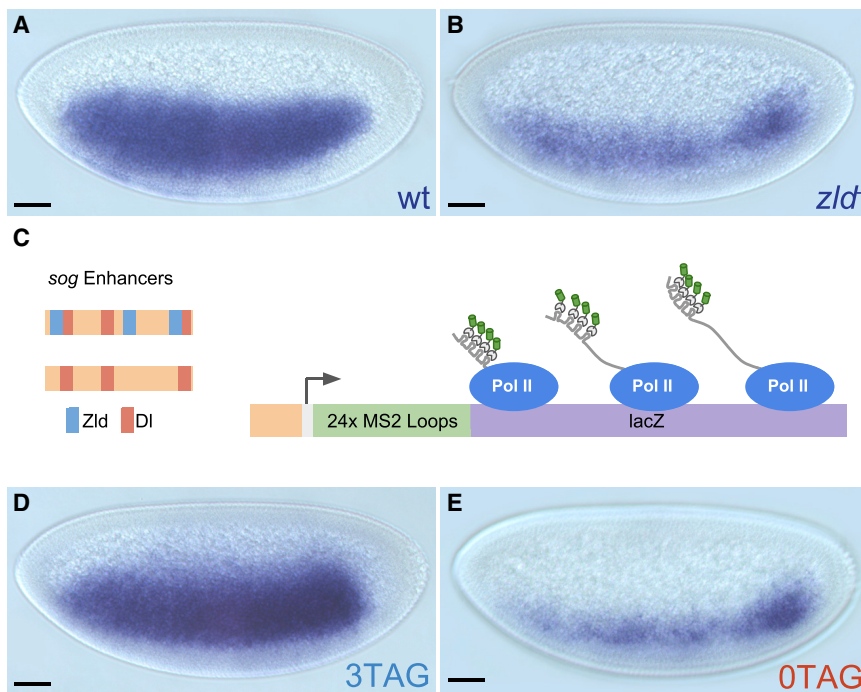


Figure 1. Zld Potentiates DI Activity at the *sog* Enhancer

(A and B) Conventional enzymatic *in situ* hybridization staining of *sog* in wild-type (A) and *zld* mutant (B) NC14 embryos.

(C) Schematic representation of transgenes. MS2 loops have been incorporated into the 5' end of the transcript upstream of a *lacZ* reporter sequence. (D and E) *In situ* hybridization staining of the engineered MS2v5(-TAG) *lacZ* transgenic embryos, showing that 3TAG (D) and 0TAG (E) expression is similar to the expression of *sog* in wild-type and *zld* mutants, respectively. Scale bar shown in bottom left corner of each embryo represents 50 μ m.

in situ experiments predict that the most dorsal zones imaged would show few active nuclei in 0TAG embryos, and this was the case. Although 3TAG embryos showed similar numbers of active nuclei in each zone across all cycles (NC12–NC14), with the exception of zone 1 in NC14 due to ventral repression by Snail (Figure 2D), in 0TAG embryos, the more dorsal the zone, the fewer the number of active nuclei (Figure 2E). Collectively, these qualitative observations are in accordance with what is currently known about how Zld participates in transcriptional activation and provide evidence that our transgenes are faithfully reporting on the transcriptional activity of *sog* in the presence or absence of Zld.

In addition to allowing qualitative assessment of transcriptional activation, MS2 reporters continually output information on the state of transcription over time, enabling an analysis of the timing of each activation event within a nuclear cycle [14]. This was performed by measuring the time between anaphase of NC12 and the appearance of fluorescent foci in NC13 and plotting the results as cumulative distribution curves (Figures 2F–2H). This analysis showed that nuclei in 3TAG embryos express simultaneously across the domain of expression (Figure 2G; Video S1). In stark contrast, we observed a significant position-dependent delay of activation in 0TAG embryos, where the ventral nuclei activate transcription well before lateral nuclei (Figure 2H; Video S2). This is presumably due to the highly dynamic nature of the DI gradient, whereby DI levels increase within and across nuclear cycles [21–23]. Here, the 0TAG reporter is effectively acting as a readout for nuclear DI concentration, suggesting that, in the absence of Zld binding sites, the *sog* enhancer responds to DI levels in a concentration-dependent manner, rather than the binary switch-like response seen in the presence of Zld.

Knowing that activation is altered in 0TAG embryos, we next examined the internal kinetic features of transcription. We

attributed to polymerases accumulating over the gene body as they transcribe the MS2 loops and continue to elongate. The length of the ramp-up phase is commonly thought of as the time in which a single polymerase molecule has traversed the entire gene body [14]. The transition to the next phase, “steady state” transcription, is reached when the rate of polymerase loading is matched by rate of polymerase unloading, diagrammed in Figure 3E. Here, the MS2 signal levels off and fluctuates within a narrow range, as there is no net gain of nascent transcripts. We have included an equation demonstrating that the signal strength at steady-state transcription can be understood as the average gap between polymerase molecules on the gene body (Figure 3E).

Using the duration of the ramp-up phase, which can be referred to as the “time to steady state,” we can calculate the number of nuclei that have reached steady-state transcription as cumulative distribution curves, with the percentage of all active nuclei at steady state plotted over time (Figures 3F and 3G). There is a striking similarity between the two genotypes, indicating that Zld does not act on the speed of polymerase. In addition, the time to steady state is similar in each of the different zones, suggesting that nuclear DI concentration has little influence on polymerase elongation rate. In contrast, when signal intensity values of steady-state transcription are averaged for each nucleus (Figure 3H), it appears that both Zld and DI are modulating the strength of transcription. Similar to our observations regarding the onset of transcriptional activation, the 3TAG reporter shows comparable max output across multiple zones until the most extreme end of the DI gradient (zone 5), whereas the 0TAG reporter shows a progressive loss of max output across the entire gradient (Figure 3F), indicating that transcriptional output rate has become a function of nuclear DI concentration. These results suggest Zld acts upstream of elongation, for example, to either increase RNA polymerase II loading or

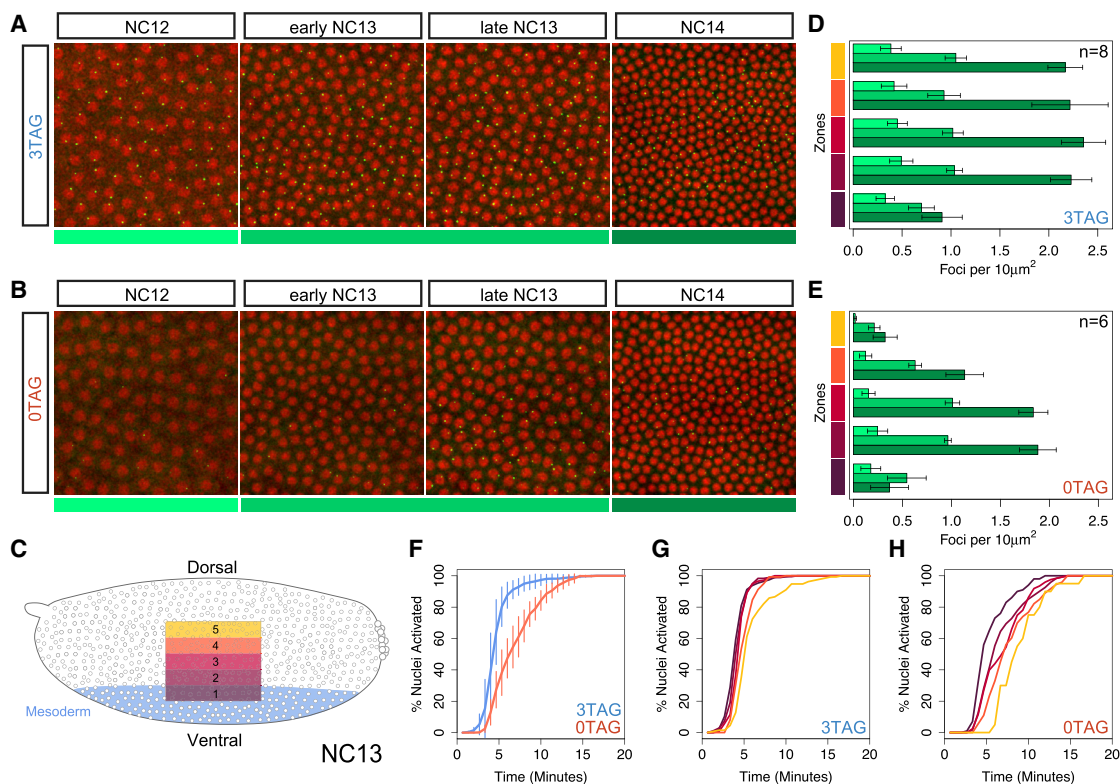


Figure 2. MS2 Imaging Reveals a Position-Dependent Transcriptional Delay in the Absence of Zld Binding Sites

(A and B) Frames taken from live imaging Videos S1 (A) and S2 (B) that track transcription (green spots) from NC12 to NC14 as indicated and color coded below, NC12 (light green), NC13 (medium green), and NC14 (dark green). Nuclei (red) have been labeled using maternally loaded H2Av-RFP.

(C) Bars on right side follow five zones along the dorsal-ventral axis with ventral mesoderm on bottom (zone 1) as diagrammed in the embryo schematic with blue shading defining the presumptive mesoderm of the embryo.

(D and E) Quantification of the number of expressing nuclei in 3TAG (D) and 0TAG (E) NC12–NC14 embryos (color coded as in A and B) agrees with conventional *in situ* analysis, showing markedly fewer active nuclei in 0TAG embryos across consecutive nuclear cycles, especially in zones 4 and 5. In total, 8 3TAG embryos and 6 0TAG embryos were analyzed as indicated in the bar plots and plotted with error bars representing one SD of all values collected for each cycle and bin. For additional videos, see Videos S3, S4, S5, and S6.

(F–H) Cumulative distribution curves of nuclei that activate transcription in NC13, excluding nuclei that never activate in NC13. Time 0 on the x axis is the start of anaphase of the previous cycle, NC12. All zones concatenated with delay values across genotypes in (F) with variance across biological replicates indicated with vertical lines showing one SD of all embryos measured. 3TAG embryos activate transcription simultaneously across the expression domain (G), and 0TAG embryos show a delay dependent on the nucleus' position in the DI gradient (H).

decrease the length of pausing experienced by a given polymerase molecule. Either of these regulatory steps would affect the mean spacing of polymerase molecules at max output.

This behavior of Zld inducing uniform transcriptional activation and output across a transcriptional activator gradient could be explained by Zld's reported ability to promote the formation of transcription factor "hubs" [10, 24, 25]. By raising the local concentration of DI at the site of transcription, Zld may effectively flatten the gradient of DI experienced by the enhancer and therefore unify the levels of transcriptional output in regions of low level DI. To test this hypothesis, we used a previously described method to examine transcription factor enrichment at sites of nascent transcript formation in *Drosophila* embryos [26, 27]. By costaining fixed embryos with an anti-DI antibody and a single molecule (sm) fluorescent *in situ* hybridization (FISH) probe targeting the *lacZ* reporter transcript [28], we could quantify the concentration of DI protein adjacent to foci of transcription. Figure 4A shows the DI gradient at comparable positions in 3TAG

and 0TAG embryos. Signal overlap between puncta of DI staining and *lacZ* staining, the presumed site of transcription, can be seen in 3D contour maps, where the surface represents the level of DI antibody signal and the site of transcription is mapped onto the texture of the contour. We classified nuclei as either having a high, mid, or low level of DI based on binning all nuclei imaged according to their average DI signal intensity, which correspond spatially to zones 1, 2, and 3 in Figures 2 and 3.

Figure 4C uses a modified approach demonstrated by Tsai et al. [29], where the radial intensity of the DI antibody stain is plotted to visualize the nuclear microenvironment that surrounds a site of active transcription (*lacZ* staining). Because the nuclear concentration of DI changes across the gradient, we divided voxel intensity by the average voxel intensity found within a nucleus. In this way, we could normalize across nuclei by defining our measurement as a unitless index describing the relative enrichment of signal at a given site of transcription, where a value of 1 indicates no enrichment. Additionally, we

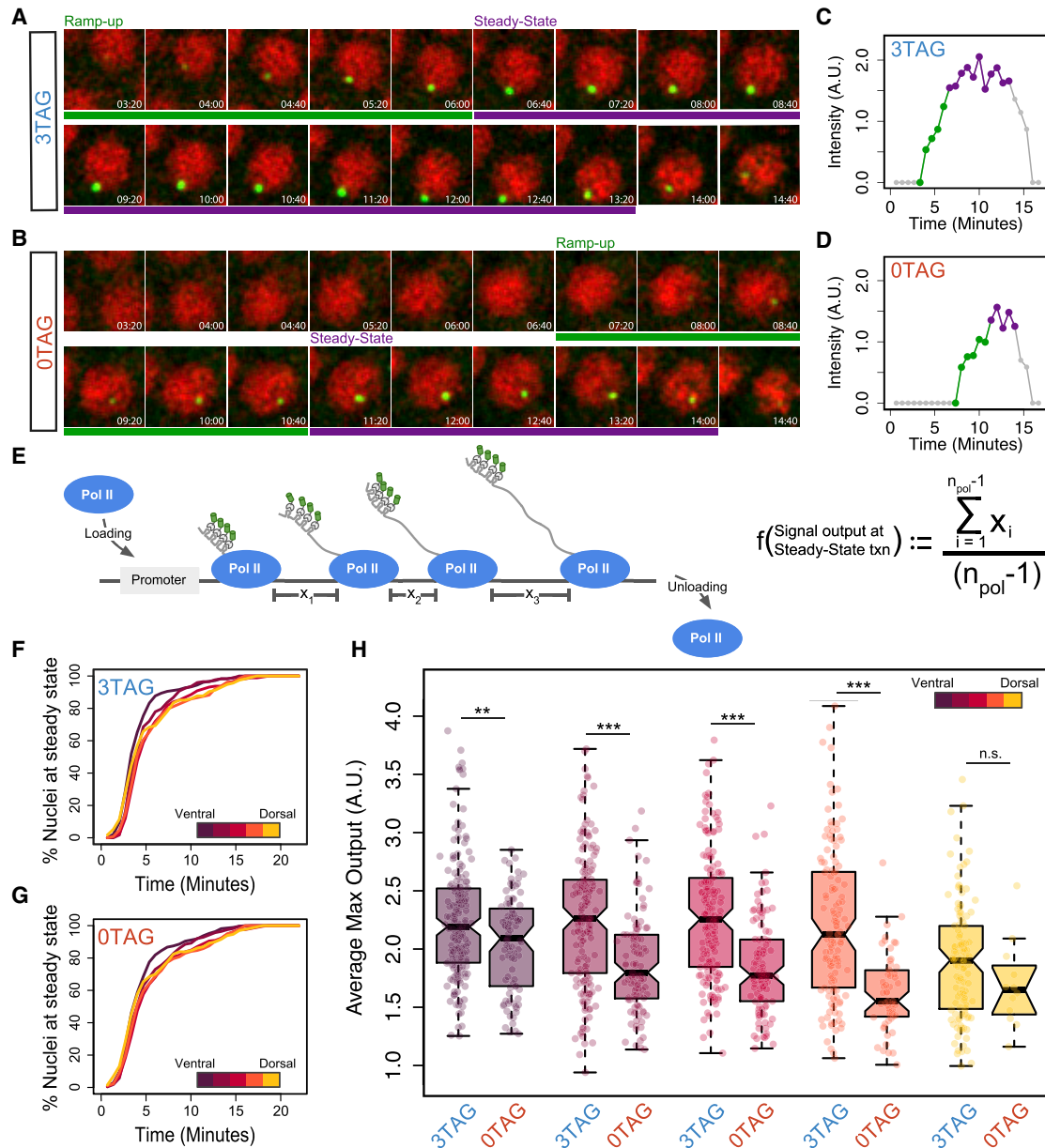


Figure 3. Zld Promotes Full Saturation of Polymerase on the Gene Body during Transcriptional Elongation

(A and B) Representative single nuclei tracked over NC13 from *Videos S1* (A) and *S2* (B). Time stamp (min) is shown in bottom right corner of each frame (time 0 is defined as the start of NC12 anaphase). Ramp-up and steady-state phases of transcription are highlighted with green and purple bars, respectively.

(C and D) Quantification of signal intensity over time in 3TAG (C) and 0TAG (D) from representative nuclei shown in (A) and (B), respectively. Phases of transcription are highlighted with corresponding colors as in (A) and (B). Ramp up is calculated as the length of time between detection above background of the MS2 focus and max output (averaged; see *STAR Methods*).

(E) Schematic representation of steady-state transcription, where the gene body is decorated with elongating RNA polymerases and the rate of loading is roughly matched by the rate of unloading. X values show the spacing between polymerase molecules. Spacing of polymerase molecules can be inferred from the signal output at steady state using the equation shown.

(F and G) Cumulative distribution curves of the percentage of nuclei that have reached steady state in different zones of 3TAG (F) and 0TAG (G) embryos.

(H) Average intensity at steady state (NC13) plotted as boxplot distributions over all five zones of the *sog* expression domain. In total for all zones, 855 and 460 nuclei were analyzed for 3TAG and 0TAG, respectively, from 8 3TAG and 6 0TAG embryos (see additional *Videos S1, S2, S3, S4, S5, and S6*). Significant differences between all zones except zone 5 were found using a Welch's t test between the genotypes. 3TAG embryos show little difference over the first four zones, and 0TAG embryos show progressive loss in signal intensity over the dorsal-ventral axis.

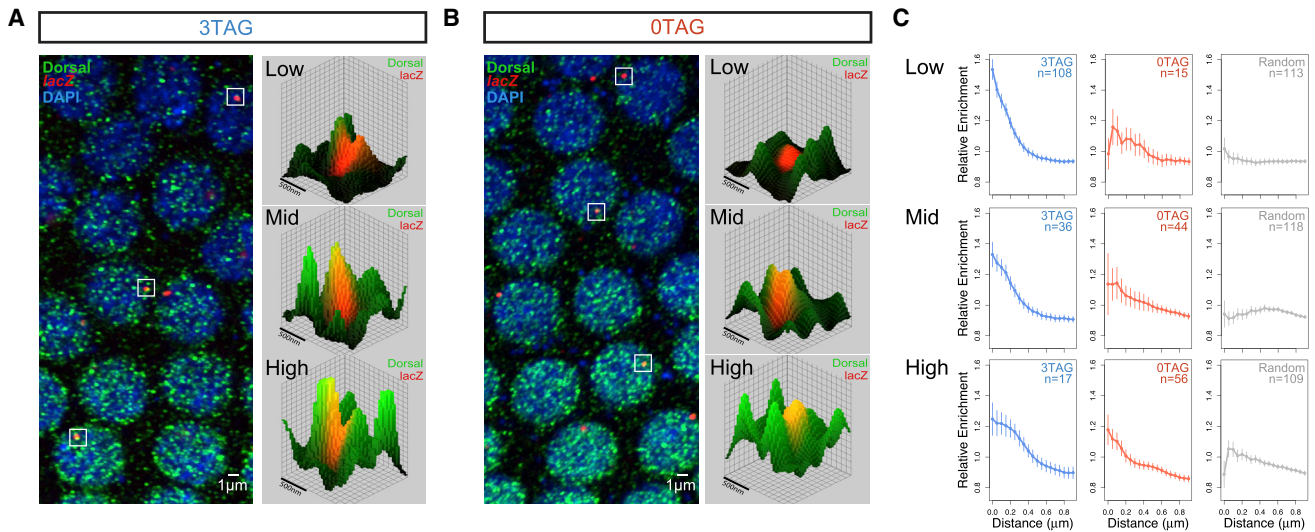


Figure 4. Zld Increases the Local Concentration of DI at the Site of Transcription

(A and B) Confocal images of NC13 embryos stained with anti-DI antibodies and smFISH probes for the *lacZ* reporter genes 3TAG (A) and 0TAG (B). DI staining appears highly punctate, indicating the possible presence of high-DI nuclear microenvironments. Sites of active transcription are visualized as red nuclear foci that can be localized in 3D space. Select foci were isolated and visualized in 3D contour maps, where the height of surface represents the intensity of the DI staining. A high incidence of FISH signal overlapping with DI microdomains was observed, suggesting the concentration of DI may have an impact on transcription. (C) The distributions of DI signal within the microdomain of transcribing foci (see Figure S1 for individual enrichment curves). In regions of high nuclear DI, both genotypes show similar distributions, but a difference is detected in regions where nuclear DI begins to drop. Control distributions were prepared using random places in the nucleus. The numbers of nuclei (n) used for the analysis are indicated. Three embryos for each genotype were used. Error bars indicate the SEM.

included a set of random points within nuclei as a control. For a full breakdown of individual enrichment curves, see Figure S1. As predicted, we see a progressive loss in enrichment over the gradient in 0TAG embryos and a measurable gain in enrichment in 3TAG embryos, indicating that Zld's ability to drive higher transcriptional output is based on enhancing the local concentration of existing transcriptional activators rather than utilizing an additional Zld-specific activation pathway. Importantly, these results strongly suggest a functional link between Zld's reported ability to induce transcription factor aggregates [10] and transcriptional output, an important first step toward a complete understanding of Zld's ability to control gene expression.

DISCUSSION

The precise logic governing *cis*-regulatory elements is still an evolving field after decades of research. The role of pioneer factors, such as Zld, in modifying chromatin has increased our understanding of how patterning transcription factors, such as DI and Bicoid (Bcd), access their target enhancers [4, 7, 8, 30, 31]; however, questions persist as to the events that occur at the site of transcription. Several recent reports have suggested that the accumulation and stable association of transcription factor aggregates, or hubs, is important for proper transcriptional output [10, 24, 25, 29]. Additionally, the *Drosophila* transcription factor Bcd is enriched in Zld hubs, particularly in nuclei with lower overall Bcd, suggesting that Zld interacts with transcription factors to raise their local concentration [24]. Our results manipulating Zld binding at the enhancer (site of transcription) agree nicely with these recent findings and for the first

time suggest a direct impact of these transcription factor hubs on transcription itself.

Our experiments identify two key parameters where Zld modifies the activity of a DI-responsive enhancer. The first parameter is the onset of transcription across the domain of *sog*, where a position-dependent delay in transcriptional activation of the reporter was observed in the 0TAG embryos. We believe that the uniformity of this response is the result of Zld's pioneering activity to ubiquitously lower the nucleosome barrier from regions of DNA in close proximity to its DNA binding motif. Freeing up enhancers may then allow DI to be bound more quickly at low concentrations, which may in turn lead to local enrichment of DI (Figure 4C). In the absence of Zld, DI must compete directly with nucleosomes to access its DNA binding sites. This competition could be more effective at high concentrations of DI, thus leading to the concentration-dependent effects observed in 0TAG. The second parameter controlled by Zld is the uniformity of the transcriptional output over the course of a nuclear cycle. Our MS2 data of 3TAG embryos showed remarkably similar levels of total transcription in all measured positions save for the most extreme dorsally located nuclei. Our results of higher DI enrichment in 3TAG embryos in nuclei with low DI tracks well with the measurements of transcription. However, it remains to be seen whether these two transcriptional parameters (timing and output) are connected by a single mechanistic step mediated by Zld binding to an enhancer.

More broadly, these experiments demonstrate the influence that Zld has on global dynamics of tissue patterning. Morphogen gradients supply positional information through an analog signal: a contiguous modulation in morphogen concentration directly encodes location along a developmental axis. When creating a

broad domain of expression from this signal, a conversion from analog to digital information must occur; a varying amount of transcriptional activator, in this case Dl, must be reliably converted into a uniform transcriptional response. Our work suggests that Dl's interaction with Zld allows it to produce near identical transcriptional output over a large range of nuclear Dl concentrations, and in the absence of that interaction, output is purely reflective of the underlying gradient. As uniform transcriptional domains that span large sections of morphogen gradients are a common motif across developmental systems, we believe our work helps shed light on a common principle of cellular fate decisions.

STAR★METHODS

Detailed methods are provided in the online version of this paper and include the following:

- KEY RESOURCES TABLE
- CONTACT FOR REAGENT AND RESOURCE SHARING
- EXPERIMENTAL MODEL AND SUBJECT DETAILS
- METHOD DETAILS
 - Depletion of maternal zld
 - Sequence of the sog 3TAG and 0TAG enhancers
 - *in situ* hybridization
 - Antibody staining
 - Construction of MS2v5(-TAG) vector
 - MS2v7 sequence (24 new loops in italics)
 - MS2v5 sequence (24 old loops in italics; Zld sites underlined)
 - Live imaging
 - High Resolution Imaging
 - Detailed Genotypes
- QUANTIFICATION AND STATISTICAL ANALYSIS

SUPPLEMENTAL INFORMATION

Supplemental Information can be found online at <https://doi.org/10.1016/j.cub.2019.03.019>.

ACKNOWLEDGMENTS

The authors would like to thank Shawn Little for the *lacZ* Atto633 smFISH probe and Sirus Mrazik and Justin Kai-Ming Yeung for help with *in situ*. We also thank Edo Kussell, Carlos Carmona-Fontaine, Grace Avecilla, and Timothee Lionnet for helpful discussions regarding quantitative analysis of MS2 data and Jonathan Liu, Jacques Bothma, and Stephen Small for insightful comments on the manuscript. The research was supported by a NIH research grant to C.A.R. (GM63024). P.H.W. was supported by a NIH training grant (5T32HD007520-20). E.C.K. was supported by the NSF GFRP. H.G.G. was supported by the Burroughs Wellcome Fund Career Award at the Scientific Interface, the Sloan Research Foundation, the Human Frontiers Science Program, the Searle Scholars Program, the Shurl & Kay Curci Foundation, the Hellman Foundation, the NIH Director's New Innovator Award (DP2 OD024541-01), and a NSF CAREER Award (1652236).

AUTHOR CONTRIBUTIONS

C.A.R., H.G.G., and P.H.W. designed the overall study. E.C.E. designed and prepared the MS2v5(-TAG) loops vector. S.Y. made the *sog* enhancer-MS2v5(-TAG) reporter constructs and carried out the live imaging experiments. C.A.R., P.H.W., and S.-K.H. carried out the assays in fixed embryos. P.H.W.

conceived the ideas and wrote code for the computational image analysis. P.H.W. wrote the draft manuscript, and all authors contributed to revisions.

DECLARATION OF INTERESTS

The authors declare no competing interests.

Received: November 14, 2018

Revised: February 7, 2019

Accepted: March 12, 2019

Published: April 11, 2019

REFERENCES

1. Steward, R., McNally, F.J., and Schedl, P. (1984). Isolation of the dorsal locus of *Drosophila*. *Nature* 311, 262–265.
2. Stathopoulos, A., and Levine, M. (2002). Dorsal gradient networks in the *Drosophila* embryo. *Dev. Biol.* 246, 57–67.
3. Liang, H.-L., Nien, C.-Y., Liu, H.-Y., Metzstein, M.M., Kirov, N., and Rushlow, C. (2008). The zinc-finger protein Zelda is a key activator of the early zygotic genome in *Drosophila*. *Nature* 456, 400–403.
4. Schulz, K.N., Bondra, E.R., Moshe, A., Villalta, J.E., Lieb, J.D., Kaplan, T., McKay, D.J., and Harrison, M.M. (2015). Zelda is differentially required for chromatin accessibility, transcription factor binding, and gene expression in the early *Drosophila* embryo. *Genome Res.* 25, 1715–1726.
5. Nien, C.-Y., Liang, H.-L., Butcher, S., Sun, Y., Fu, S., Gocha, T., Kirov, N., Manak, J.R., and Rushlow, C. (2011). Temporal coordination of gene networks by Zelda in the early *Drosophila* embryo. *PLoS Genet.* 7, e1002339.
6. Harrison, M.M., and Eisen, M.B. (2015). Transcriptional activation of the zygotic genome in *Drosophila*. *Curr. Top. Dev. Biol.* 113, 85–112.
7. Foo, S.M., Sun, Y., Lim, B., Ziukaite, R., O'Brien, K., Nien, C.-Y., Kirov, N., Shvartsman, S.Y., and Rushlow, C.A. (2014). Zelda potentiates morphogen activity by increasing chromatin accessibility. *Curr. Biol.* 24, 1341–1346.
8. Sun, Y., Nien, C.-Y., Chen, K., Liu, H.-Y., Johnston, J., Zeitlinger, J., and Rushlow, C. (2015). Zelda overcomes the high intrinsic nucleosome barrier at enhancers during *Drosophila* zygotic genome activation. *Genome Res.* 25, 1703–1714.
9. Harrison, M.M., Li, X.-Y., Kaplan, T., Botchan, M.R., and Eisen, M.B. (2011). Zelda binding in the early *Drosophila melanogaster* embryo marks regions subsequently activated at the maternal-to-zygotic transition. *PLoS Genet.* 7, e1002266.
10. Mir, M., Reimer, A., Haines, J.E., Li, X.Y., Stadler, M., Garcia, H., Eisen, M.B., and Darzacq, X. (2017). Dense Bicoid hubs accentuate binding along the morphogen gradient. *Genes Dev.* 31, 1784–1794.
11. Kanodia, J.S., Liang, H.-L., Kim, Y., Lim, B., Zhan, M., Lu, H., Rushlow, C.A., and Shvartsman, S.Y. (2012). Pattern formation by graded and uniform signals in the early *Drosophila* embryo. *Biophys. J.* 102, 427–433.
12. Larson, D.R., Zenklusen, D., Wu, B., Chao, J.A., and Singer, R.H. (2011). Real-time observation of transcription initiation and elongation on an endogenous yeast gene. *Science* 332, 475–478.
13. Forrest, K.M., and Gavis, E.R. (2003). Live imaging of endogenous RNA reveals a diffusion and entrapment mechanism for nanos mRNA localization in *Drosophila*. *Curr. Biol.* 13, 1159–1168.
14. Garcia, H.G., Tikhonov, M., Lin, A., and Gregor, T. (2013). Quantitative imaging of transcription in living *Drosophila* embryos links polymerase activity to patterning. *Curr. Biol.* 23, 2140–2145.
15. Lucas, T., Ferraro, T., Roelens, B., De Las Heras Chanes, J., Walczak, A.M., Coppey, M., and Dostatni, N. (2013). Live imaging of bicoid-dependent transcription in *Drosophila* embryos. *Curr. Biol.* 23, 2135–2139.
16. Lucas, T., Tran, H., Perez Romero, C.A., Guillou, A., Fradin, C., Coppey, M., Walczak, A.M., and Dostatni, N. (2018). 3 minutes to precisely measure morphogen concentration. *PLoS Genet.* 14, e1007676.

17. Wu, B., Miskolci, V., Sato, H., Tutucci, E., Kenworthy, C.A., Donnelly, S.K., Yoon, Y.J., Cox, D., Singer, R.H., and Hodgson, L. (2015). Synonymous modification results in high-fidelity gene expression of repetitive protein and nucleotide sequences. *Genes Dev.* *29*, 876–886.
18. Hong, J.-W., Hendrix, D.A., and Levine, M.S. (2008). Shadow enhancers as a source of evolutionary novelty. *Science* *321*, 1314.
19. Ozdemir, A., Ma, L., White, K.P., and Stathopoulos, A. (2014). Su(H)-mediated repression positions gene boundaries along the dorsal-ventral axis of *Drosophila* embryos. *Dev. Cell* *31*, 100–113.
20. Saint, R., and Clarkson, M. (2000). Pictures in cell biology. A functional marker for *Drosophila* chromosomes in vivo. *Trends Cell Biol.* *10*, 553.
21. Kanodia, J.S., Rikhy, R., Kim, Y., Lund, V.K., DeLotto, R., Lippincott-Schwartz, J., and Shvartsman, S.Y. (2009). Dynamics of the Dorsal morphogen gradient. *Proc. Natl. Acad. Sci. USA* *106*, 21707–21712.
22. Liberman, L.M., Reeves, G.T., and Stathopoulos, A. (2009). Quantitative imaging of the Dorsal nuclear gradient reveals limitations to threshold-dependent patterning in *Drosophila*. *Proc. Natl. Acad. Sci. USA* *106*, 22317–22322.
23. Reeves, G.T., Trisnadi, N., Truong, T.V., Nahmad, M., Katz, S., and Stathopoulos, A. (2012). Dorsal-ventral gene expression in the *Drosophila* embryo reflects the dynamics and precision of the dorsal nuclear gradient. *Dev. Cell* *22*, 544–557.
24. Mir, M., Stadler, M.R., Ortiz, S.A., Hannon, C.E., Harrison, M.M., Darzacq, X., and Eisen, M.B. (2018). Dynamic multifactor hubs interact transiently with sites of active transcription in *Drosophila* embryos. *eLife* *7*, e40497.
25. Dufourt, J., Trullo, A., Hunter, J., Fernandez, C., Lazaro, J., Dejean, M., Morales, L., Nait-Amer, S., Schulz, K.N., Harrison, M.M., et al. (2018). Temporal control of gene expression by the pioneer factor Zelda through transient interactions in hubs. *Nat. Commun.* *9*, 5194.
26. He, F., Ren, J., Wang, W., and Ma, J. (2011). A multiscale investigation of bicoid-dependent transcriptional events in *Drosophila* embryos. *PLoS ONE* *6*, e19122.
27. Xu, H., Sepúlveda, L.A., Figard, L., Sokac, A.M., and Golding, I. (2015). Combining protein and mRNA quantification to decipher transcriptional regulation. *Nat. Methods* *12*, 739–742.
28. Little, S.C., Tikhonov, M., and Gregor, T. (2013). Precise developmental gene expression arises from globally stochastic transcriptional activity. *Cell* *154*, 789–800.
29. Tsai, A., Muthusamy, A.K., Alves, M.R., Lavis, L.D., Singer, R.H., Stern, D.L., and Crocker, J. (2017). Nuclear microenvironments modulate transcription from low-affinity enhancers. *eLife* *6*, e28975.
30. Li, X.-Y., and Eisen, M.B. (2018). Zelda potentiates transcription factor binding to zygotic enhancers by increasing local chromatin accessibility during early *Drosophila melanogaster* embryogenesis. *bioRxiv*. <https://doi.org/10.1101/380857>.
31. Xu, Z., Chen, H., Ling, J., Yu, D., Struffi, P., and Small, S. (2014). Impacts of the ubiquitous factor Zelda on Bicoid-dependent DNA binding and transcription in *Drosophila*. *Genes Dev.* *28*, 608–621.
32. Groth, A.C., Fish, M., Nusse, R., and Calos, M.P. (2004). Construction of transgenic *Drosophila* by using the site-specific integrase from phage phiC31. *Genetics* *166*, 1775–1782.
33. Bischof, J., Maeda, R.K., Hediger, M., Karch, F., and Basler, K. (2007). An optimized transgenesis system for *Drosophila* using germ-line-specific phiC31 integrases. *Proc. Natl. Acad. Sci. USA* *104*, 3312–3317.
34. Hertz, G.Z., and Stormo, G.D. (1999). Identifying DNA and protein patterns with statistically significant alignments of multiple sequences. *Bioinformatics* *15*, 563–577.
35. Francois, V., Solloway, M., O'Neill, J.W., Emery, J., and Bier, E. (1994). Dorsal-ventral patterning of the *Drosophila* embryo depends on a putative negative growth factor encoded by the short gastrulation gene. *Genes Dev.* *8*, 2602–2616.

STAR★METHODS

KEY RESOURCES TABLE

REAGENT or RESOURCE	SOURCE	IDENTIFIER
Antibodies		
Sheep anti-DIG-AP antibody	Roche	Cat# 11093274910, RRID:AB_2734716
Mouse anti-DL antibody (7A4)	Developmental Studies Hybridoma Bank	Cat# anti-Dorsal 7A4, RRID:AB_528204
Alexa fluor 488 goat anti mouse secondary antibody	ThermoFisher Scientific	Cat# A-11001, RRID:AB_2534069
Chemicals, Peptides, and Recombinant Proteins		
5-Bromo-4-chloro-3-indolyl phosphate p-toluidine salt(BCIP)	Roche	Cat# 10760994001
4-Nitro blue tetrazolium chloride(NBT)	Roche	Cat# 11585029001
DIG RNA labeling mix	Roche	Cat# 11277073910
RNA FISH Hybridization Buffer	Stellaris (LGC Biosearch Technologies)	Cat# SMF-HB1-10
DAPI	Sigma-Aldrich	Cat# D9542
Aqua-Poly/Mount	Polysciences	Cat# 18606-20
Number 1.5 glass coverslips	Fisher Scientific	Cat# 22266858
Gibson Assembly Master Mix	New England Biolabs, Inc	Cat# E2611S
<i>lacZ</i> Atto633 smFISH Probe	Shawn Little's lab	[28]
<i>lacZ</i> ISH DIG RNA Probe	This lab	
<i>sog</i> ISH DIG RNA Probe	This lab	
Experimental Models: Drosophila Strains		
<i>y[1] w[1118]</i>	Bloomington Drosophila Stock Center	Cat# 6598
<i>y[1] w[*]; P{w[+mC] = His2Av-mRFP1}II.2; P{w[+mC] = nos-MCP.EGFP}2</i>	Bloomington Drosophila Stock Center	Cat# 60340, RRID:BDSC_60340
Maternal Triple Driver(MTD)-Gal4: P{COG-GAL4:VP16}; P{Gal4-nos.NGT}40; P{nos-Gal4-VP16}	Bloomington Drosophila Stock Center	Cat# 31777, RRID:BDSC_31777
UAS-shRNA- <i>zld</i>	This lab	[8]
<i>sog</i> 3TAG-MS2- <i>lacZ</i>	This paper	N/A
<i>sog</i> 0TAG-MS2- <i>lacZ</i>	This paper	N/A
Recombinant DNA		
<i>pib-evepr-ms2v5(-TAG)-lacZ</i> plasmid	This paper	N/A
Software and Algorithms		
FIJI (ImageJ)	NIH	http://fiji.sc
MATLAB	The Mathworks Inc.	https://www.mathworks.com
Imaris	Bitplane	http://www.bitplane.org
R	The R Foundation	https://www.r-project.org
LAS X	Leica Microsystems Inc	https://www.cellularimaging.nl/leica-las-x/
N2012	CarlZE Zeiss Inc	https://www.zeiss.com/corporate/int/home.html
Other		
Confocal microscope	Leica	SP8
Confocal microscope	Zeiss	LSM 880
Microscope	Zeiss	Axioskop
Digital camera for microscopy	Zeiss	AxioCam MRc
Power meter(X-cite)	Lumen Dynamics Group Inc, Canada	Model # XR2100
Breathable membrane (Lumox Film)	Sarstedt AG & Co.; Nümbrecht, Germany	Cat# 94.6077.317
Plastic microscope slide (3D printed)	Sculpteo; Créteil, France	N/A

CONTACT FOR REAGENT AND RESOURCE SHARING

Requests for any information and requests for resources or reagents should be directed to the Lead Contact, Christine Rushlow (car2@nyu.edu).

EXPERIMENTAL MODEL AND SUBJECT DETAILS

All flies were grown on standard fly (*Drosophila melanogaster*) cornmeal-molasses-yeast media. *y[1]w[1118]* (used as wild-type flies), *zld* shmir (*zld*^Δ) (see “Depletion of maternal *zld*” section below) [8], and transgenic embryos (3TAG and 0TAG) were collected on yeasted grape juice agar plates. Flies of the genotype *y[1] w⁺; P{His2Av-mRFP1}II.2; P{nos-MCP.EGFP}2* (Bloomington Stock Number 60340) carried two transgenes, one on chromosome 3, *P{nos-MCP.EGFP}2*, which expresses the MS2 coat protein (MCP) fused to EGFP under the control of the *nanos* promoter active in oogenesis, and the other on chromosome 2, *P{His2Av-mRFP1}II.2*, which expresses RFP-tagged His2Av in all cells under the control of *His2Av*. MS2 transgenes were constructed in the following manner: MS2 loop sequences were revised since previously used MS2 loops [12–14, 16, 17] contained potential Zld binding sites [5, 14, 16]. The new MS2 loops sequence, MS2v5(-TAG) (see Method Details for DNA sequence) was placed in between the *eve* minimal promoter and a *lacZ* reporter gene (*pib-evepr-ms2v5(-TAG)-lacZ* plasmid), then subcloned into an attB vector (pBPhi) containing *sog* enhancers with (3TAG) or without (0TAG) Zld binding sites [7] (Method Details). Transgenic lines carrying these constructs were generated by phiC31 integration in the 53B2 landing site (VK00018), Bloomington stock number 9736 [32, 33] by BestGene.

METHOD DETAILS

Depletion of maternal *zld*

Embryos were collected from females depleted of *zld* RNAs by RNAi prepared in two crosses [8]: 1st cross ♀ +; +; UAS-shRNA-*zld* X ♂ P{COG-GAL4:VP16}; P{Gal4-*nos*.NGT}40; P{*nos*-Gal4-VP16}; 2nd cross G1♀ P{COG-GAL4:VP16}/+; P{Gal4-*nos*.NGT}40/+; P{*nos*-Gal4-VP16}/ UAS-shRNA-*zld* X ♂ *yw*

Sequence of the *sog* 3TAG and 0TAG enhancers

sog 3TAG

426 bp enhancer sequence (Zld binding sites underlined):

GTTTCAGCGGAACAGGTAGGCTGGTCGATCGGAAATCCCACCATACACATGTGGCTATAATGCCAACGGCATCGAGGTGCGA
AAACAGATGCAGCCTCATAAAAGGGGCGCAGATAAGGTGCGGTTGCGTGGGAAAAGCCCATCCGACCAGGACCAGGACGAAG
CAGTGC GGTTGGCGCATCATTGCCGCCATATCTGCTATTCTACCTGCGTGGCCATGGCGATATCCTTGTGCAAGGATAAGGAGC
GGGGATCATAAAACGCTGTGCTTTTGTATGCTGCTATTAAATTGGCTTCTTGGCGGGCGTTGCAACCTGGTGCTAGTCCCA
ATCCCAATCCCAATTCCAATCCCAATCCATATACCATATCCAATGCATTCTACCTGTCTCTGGGAATTTCCGATCTGGCCGCACCCATAT

sog 0TAG

426 bp enhancer sequence (mutated Zld binding sites underlined):

GTTTCAGCGGAACCAACAAGCTGGTCGATCGGAAATCCCACCATACACATGTGGCTATAATGCCAACGGCATCGAGGTGCG
AAAACAGATGCAGCCTCATAAAAGGGGCGCAGATAAGGTGCGGTTGCGTGGGAAAAGCCCATCCGACCAGGACCAGGACGAAG
GCAGTGC GGTTGGCGCATCATTGCCGCCATATCTGCTATTCTTGTGGCGTGGCCATGGCGATATCCTTGTGCAAGGATAAGGA
GCGGGGATCATAAAACGCTGTGCTTTTGTATGCTGCTATTAAATTGGCTTCTTGGCGGGCGTTGCAACCTGGTGCTAGTGC
CCAATCCCAATCCCAATTCCAATCCCAATCCATATACCATATCCAATGCATTTTGTGGTCTCTGGGAATTTCCGATCTGGCCGCA
CCCATAT

in situ hybridization

Embryos were collected and aged to be 1–3 hours old at room temperature and dechorionated in Clorox for two minutes. They were then fixed in 4% formaldehyde (1X PBS) and an equal volume of heptane for 25 minutes while shaking vigorously. Devitellinization was performed by pipetting off the bottom fixative phase and adding 4 mL of methanol and shaking vigorously for 30 s. Embryos were rinsed in methanol and transferred to ethanol for storage at –20°C. Hybridization of fixed embryos used a standard *in situ* hybridization (ISH) protocol and DIG-labeled *sog* cDNA or *lacZ* RNA antisense probes [7]; hybridized at 55°C overnight). Visualization of the labeled probe was done using anti-DIG-AP (alkaline phosphatase) antibodies (Roche Biochemicals) followed by histochemical enzymatic staining reagents (Roche Biochemicals). For smFISH, Atto-633 conjugated probe sets complementary to *lacZ* (gift from Shawn Little) [28] were used in hybridization experiments using Stellaris (LGC Biosearch Technologies) reagents and protocols.

Antibody staining

Antibody staining was performed at 4°C for 16 hours followed by three 20 minute washes in PBS + 0.1% Tris pH 7.0. Anti-DI antibody (DI_7A4) was obtained from the Developmental Studies Hybridoma Bank and used at 1:50 dilution. Embryos were then stained with

power was set at 1% (405nm), 5% (488nm), 15% (633nm). All images were captured using the the Airyscan detector array. Post-processing was carried out using the ZEN2012 software “Airyscan Processing” feature.

Detailed Genotypes

Figure 1

1A: wt = ♀ *y[1] w[*]* X ♂ *y[1] w[*]*
 1B: *zld* prepared by *zld* RNAi in two crosses: 1st cross ♀ +; +; UAS-shRNA-*zld* X ♂ P{COG-GAL4:VP16}; P{Gal4-nos.NGT}40; P{nos-Gal4-VP16}; 2nd cross G1♀ P{COG-GAL4:VP16}/+; P{Gal4-nos.NGT}40/+; P{nos-Gal4-VP16}/ UAS-shRNA-*zld* X ♂ *yw*
 1D: 3TAG = *y[1] w[*]*; *sog* 3TAG-MS2-*lacZ*;+
 1E: 0TAG = *y[1] w[*]*; *sog* 0TAG-MS2-*lacZ*;+

Figure 2

2A, 2C, and 2E: 3TAG ♀ *y[1] w[*]*; P{w[+mC] = His2Av-mRFP1}II.2; P{w[+mC] = nos-MCP.EGFP}2 X ♂ *y[1] w[*]*; *sog* 3TAG-MS2-*lacZ*;+
 2B, 2D, and 2F: 0TAG ♀ *y[1] w[*]*; P{w[+mC] = His2Av-mRFP1}II.2; P{w[+mC] = nos-MCP.EGFP}2 X ♂ *y[1] w[*]*; *sog* 0TAG-MS2-*lacZ*;+

Figure 3

3B, 3D, and 3F: 3TAG ♀ *y[1] w[*]*; P{w[+mC] = His2Av-mRFP1}II.2; P{w[+mC] = nos-MCP.EGFP}2 X ♂ *y[1] w[*]*; *sog* 3TAG-MS2-*lacZ*;+
 3C, 3E, and 3F: 0TAG ♀ *y[1] w[*]*; P{w[+mC] = His2Av-mRFP1}II.2; P{w[+mC] = nos-MCP.EGFP}2 X ♂ *y[1] w[*]*; *sog* 0TAG-MS2-*lacZ*;+

Figure 4

4A, 4B, and 4C: 3TAG *y[1] w[*]*; *sog* 3TAG-MS2-*lacZ*;+
 4A, 4B, and 4C: 0TAG *y[1] w[*]*; *sog* 0TAG-MS2-*lacZ*;+

Figure S1 (Related to Figure 4)

S1A, S1C, and S1D: 3TAG *y[1] w[*]*; *sog* 3TAG-MS2-*lacZ*;+
 S1B, S1C, and S1D: 0TAG *y[1] w[*]*; *sog* 0TAG-MS2-*lacZ*;+

Videos (Related to Figures 2 and 3)

Videos S1, S3, and S5: 3TAG *y[1] w[*]*; *sog* 3TAG-MS2-*lacZ*;+
 Videos S2, S4, and S6: 0TAG *y[1] w[*]*; *sog* 0TAG-MS2-*lacZ*;+

QUANTIFICATION AND STATISTICAL ANALYSIS

Live imaging Videos (Videos S1, S2, S3, S4, S5, and S6) were analyzed using the Imaris (Bitplane, Oxford Instruments, Concord MA) “spots” function over and track using retrograde motion with a max frame gap of 3. MS2 foci were assumed to be 1 μ m across with a z axis point spread function estimation of 2 μ m. After tracking, both intensity sum and position csv files were exported and analyzed using a series of custom R scripts. Tracks are assigned a nuclear cycle and zone position by referencing a manually generated annotation file containing all frames where anaphase was reached for each Video and a y axis position of ventral repression at nuclear cycle 14. Transcriptional delay values for each tracked object were generated by subtracting the current frame number by the preceding anaphase frame number. Transcriptional dynamics at different dorsal-ventral positions was analyzed by subdividing each image into five zones along the DV axis. Zone 1 comprises the mesoderm, as determined by the Snail repression border that becomes obvious in early NC14. The remaining zones are defined by 20 μ m spatial bins that proceed dorsally, approximately 4 rows of nuclei per zone (schematized in Figure 2C).

To measure transcriptional kinetic parameters, we used individual foci and performed a linear fit on the first 25% of the intensity values over time. Time to steady-state values were calculated by intersecting the linear fit with a horizontal line generated by the averaging the top 20% of intensity values for foci signals. Statistical tests were performed using Welch’s t test that assumes independent underlying variance. P values shown in Figure 3H are visually represented as one asterisk indicating a $p < 0.05$, two indicating $p < 0.01$, and three indicating $p < 0.001$.

The smFISH nascent transcript values shown in Figure 4 were obtained by extracting the total fluorescence of large nuclear localized foci assumed to be the point of active transcription. This value was then divided by intensity values of single transcripts by assuming an average 0.3 μ m diffraction limited point again using the Imaris “spots.” These values formed a normal distribution

from which the median value was selected as the fluorescence intensity value of a single transcript within a single frame. DI intensity values for each nucleus were found by extracting the mean fluorescence of antibody stain signal within volumes defined by nuclear DAPI signal. This normalizes differences in DI concentrations along the gradient between genotypes. Radial scans were performed using a custom R script that utilized the position values extracted from Imaris to interrogate .tif files of the DI antibody stain. Error bars on enrichment plots in [Figure 4C](#) are standard error of the mean of individual enrichment curves in each positional bin. All plotting was performed with base R functions and the ggplot2 library.

Current Biology, Volume 29

Supplemental Information

**The *Drosophila* Pioneer Factor Zelda Modulates
the Nuclear Microenvironment of a Dorsal Target
Enhancer to Potentiate Transcriptional Output**

Shigehiro Yamada, Peter H. Whitney, Shao-Kuei Huang, Elizabeth C. Eck, Hernan G. Garcia, and Christine A. Rushlow

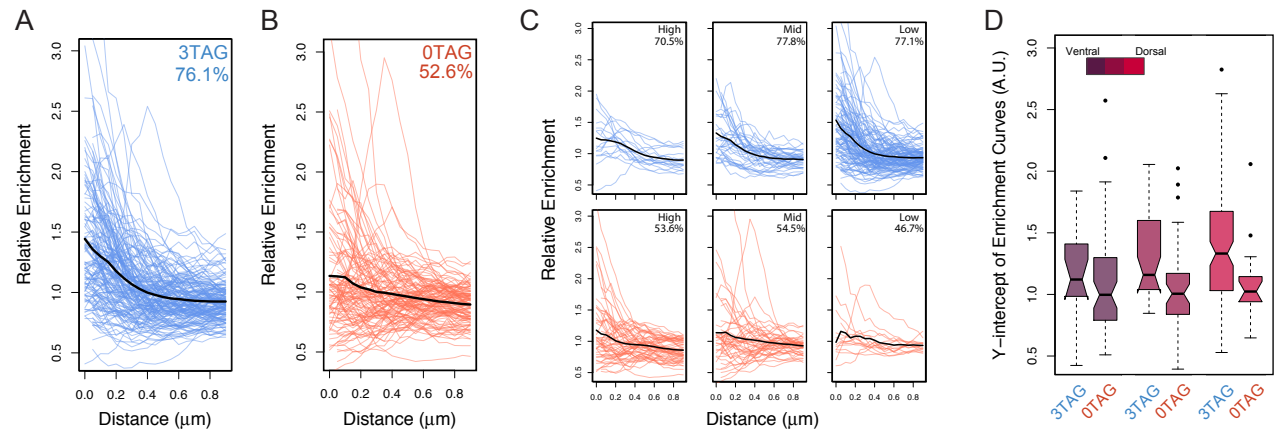


Figure S1. DI enrichment at the 3TAG enhancer increases across the D/V axis. Related to Figure 4.

(A-B) Individual enrichment curves plotted together for each genotype, as indicated. Average enrichment profiles of all curves are plotted in black. Percentages show the fraction of curves that have a y-intercept greater than 1, indicating the proportion of nuclei that show net enrichment. (C) Individual enrichment curves from each bin plotted in the same manner; 3TAG on top (blue), 0TAG on bottom (red). Note that the y-intercept of the 3TAG foci increases as the nuclear concentration of DI falls, which explains how we can observe uniform transcriptional output across the gradient in 3TAG, i.e., DI is more enriched in regions where there is less nuclear DI, thereby maintaining uniform output. However, the median value of 0TAG foci stays relatively flat at 1.0 across the gradient as expected since there is no enrichment without Zld. Note also that the percentages of enriched lines, which are the lines with a y-intercept greater than 1 (indicated in the upper right corner of each panel) do not appreciably change over the DI gradient for either genotype, therefore the effect of enrichment is restricted to the amplitude of enrichment rather than the percentage of cells that are enriched. (D) Boxplots showing the distribution of y-intercepts from each spatial bin.